

Bright Luminescent Surface States on the Edges of Wide-bandgap Two-dimensional Lead Halide Perovskite

Yanan Wang,^{1,3,†,¥} Chong Wang,^{2,3,†} Xinghua Su,^{4,3,†} Viktor G. Hadjiev,^{5,6} Hector A Calderon Benavides⁷
Yizhou Ni,^{5,8} Md Kamrul Alam,⁹ Francisco C. Robles-Hernandez,^{10,3} Yan Yao,^{3,5,9} Shuo Chen,^{5,8} Zhiming
Wang,^{1,*} Jiming Bao^{3,1,9,*}

¹Institute of Fundamental and Frontier Sciences, University of Electronic Science and Technology of China, Chengdu, Sichuan 610054, China

²Institute of Optoelectronic Information Material, School of Material Science and Engineering, Yunnan University, Kunming, Yunnan 650091, China

³Department of Electrical and Computer Engineering, University of Houston, Houston, Texas 77204, United States

⁴School of Materials Science and Engineering, Chang'an University, Xi'an, Shaanxi 710061, China

⁵Texas Center for Superconductivity, University of Houston, Houston, TX 77204, United States

⁶Department of Mechanical Engineering, University of Houston, Houston, TX 77204, United States

⁷Instituto Politecnico Nacional, ESFM-IPN, UPALM, Departamento de Física, Mexico CDMX 07338, Mexico

⁸Department of Physics, University of Houston, Houston, Texas 77204, United States

⁹Materials Science & Engineering, University of Houston, Houston, Texas 77204, United States

¹⁰Mechanical Engineering Technology, University of Houston, Houston, TX 77204, United States

[†]Equal contributions

*Corresponding author. E-mail: jbao@uh.edu (J.M.B.); zhmwang@uestc.edu.cn (Z.M.W.)

¥Current address: Electrical Engineering & Computer Science, Case Western Reserve University, Cleveland, Ohio 44106, United States

Abstract

Three-dimensional lead halide perovskites have surprised people for their defect-tolerant electronic and optical properties, two-dimensional lead halide layered structures exhibit even more puzzling phenomena: luminescent edge states in Ruddlesden-Popper perovskites and conflicting reports of highly luminescent versus non-emissive CsPb_2Br_5 . In this work, we report the observation of bright luminescent surface states on the edges of CsPb_2Br_5 microplatelets. We prove that green surface emission makes wide-bandgap single crystal CsPb_2Br_5 highly luminescent. Using polarized Raman spectroscopy and atomic-resolution transmission electron microscopy, we further prove that polycrystalline CsPb_2Br_5 is responsible for the bright luminescence. We propose that these bright edge states originate from corner-sharing clusters of PbBr_6 in the distorted regions between CsPb_2Br_5 nanocrystals. Because metal halide octahedrons are building block of perovskites, our discoveries settle a long-standing controversy over the basic property of CsPb_2Br_5 and open new opportunities to understand, design and engineer perovskite solar cells and other optoelectronic devices.

Lead halide perovskites have provided us not only an ideal material platform to realize the dream of high-efficiency solar cells and many other optoelectronic devices, but also a wide range of structures to explore unusual fundamental sciences^{1, 2, 3, 4}. Depending on spatial configurations, lead halide octahedrons can form structures from three dimensional (3D) all the way to 0D perovskites⁵. While still not completely understood, the superior optoelectronic properties of perovskites are believed to originate from their immunity to defects and lack of non-radiative deep level traps. More surprising is recent observation of highly emissive deep-level states on the edges of 2D Ruddlesden-Popper (R-P) $(\text{BA})_2(\text{MA})_{n-1}\text{Pb}_n\text{I}_{3n+1}$ perovskites and subsequent utilization of such edge state to further enhance the efficiency of solar cells⁶. However, the nature of the edge states is not clear, and evens their chemical composition and microscopic structure have not been identified⁶.

CsPb_2Br_5 is another type of layered lead halide structure with edge-shared PbBr_6 octahedrons forming flat sheets and Cs as spacing layers. 2D CsPb_2Br_5 has also attracted a lot of attention recently due to many conflicting reports on its luminescence although it was synthesized and studied long ago^{7, 8}. Zhang et al. were the first to report the beneficial effect of CsPb_2Br_5 to a 3D all-inorganic perovskite CsPbBr_3 : the attachment of CsPb_2Br_5 nanoparticles to CsPbBr_3 nanocrystals enhanced photoluminescence (PL) of CsPbBr_3 by several folds and external quantum efficiency of CsPbBr_3 light-emitting diodes (LEDs) by 50%⁹. Shortly after that, Wang and co-workers reported nearly 90% quantum efficiency of pure CsPb_2Br_5 nanoplatelets and subsequently expanded their emission wavelength to whole visible spectrum using ion exchange with I and Cl¹⁰. But these claims of highly luminescent CsPb_2Br_5 have been met with skeptics. Li *et al.* observed no PL at all and further proved it as an indirect wide bandgap semiconductor with theoretical support from density functional theory (DFT) simulation¹¹. Since then, the controversy has remained, while some groups still reported strong visible photoluminescence, high efficiency LEDs, photodetectors, and even lasing action in CsPb_2Br_5 microplates^{12, 13, 14, 15, 16, 17}, others supported the opposite, believing PL due to embedded CsPbBr_3 ^{18, 19}. Many groups were aware of this controversy but were not able to support either of these two opposing claims^{20, 21, 22}.

Edges are intrinsic surfaces of two-dimensional materials, and typically are sources for defects that can greatly degrade device performances. Here we report the observation of bright photoluminescence from the edges of CsPb₂Br₅ microplatelets and prove that polycrystalline CsPb₂Br₅ is responsible for luminescent edge states of non-luminescent wide-bandgap single crystal CsPb₂Br₅. This discovery is made possible by our unique synthesis and characterization techniques. Pure water is the only chemical needed for the synthesis of CsPb₂Br₅ from CsPbBr₃. CsPb₂Br₅ microplatelets with different edge morphologies are obtained such that edge emissions can be spatially located and distinguished from the body emission. Polarization-dependent micro-Raman in conjunction with micro-PL and atomic-resolution transmission electron microscopy (TEM) allows us to correlate luminescent sources to the underlying crystal structure. In-situ PL imaging of water-induced CsPbBr₃ to CsPb₂Br₅ phase transformation and combined Raman/PL of water-immersed CsPb₂Br₅ further exclude CsPbBr₃ as a luminescent source. Our discoveries settle the debate on the basic properties of CsPb₂Br₅ and pave the way for further exploration, understanding and device applications of a wide range of lead halide perovskites.

CsPbBr₃ powders were first synthesized using a modified method by mixing 0.5 M Pb(CH₃COO)₂·3H₂O and 1 M CsBr in 48% HBr solution at room temperature^{23, 24}. CsPb₂Br₅ was then synthesized by simply dropping CsPbBr₃ micropowders in a large quantity of water in a flask (20-50 times more water in mass) at room temperature. Orange CsPbBr₃ quickly turned white and precipitated at the bottom of the flask. The white precipitates can be taken out and dried for further study. The very pure phases of initial CsPbBr₃ and precipitated CsPb₂Br₅ were verified by their clean XRD patterns.

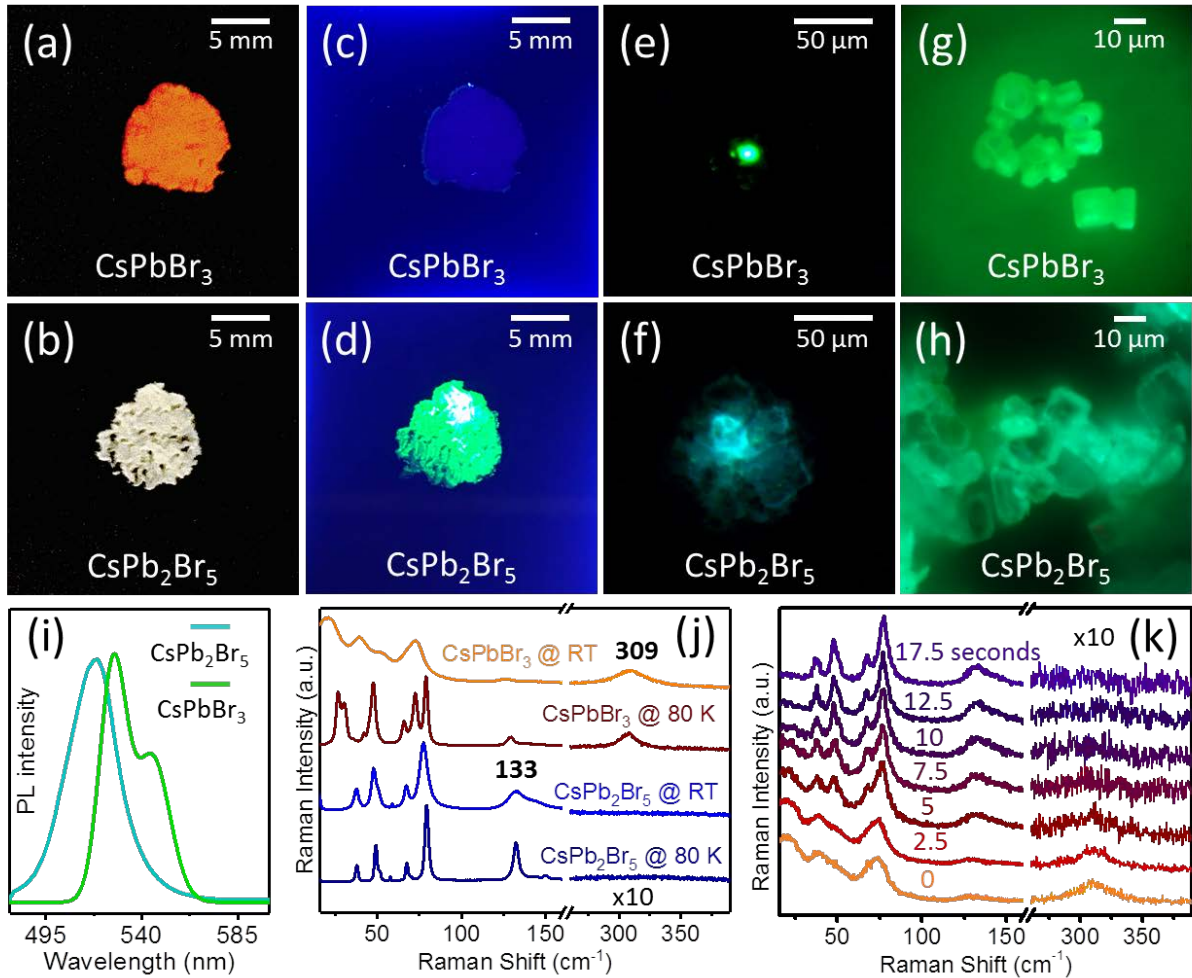


Fig. 1. Optical and luminescence images of CsPbBr₃ and CsPb₂Br₅ as well as their Raman and photoluminescence spectra. (a-d) Pictures of CsPbBr₃ and CsPb₂Br₅ under (a-b) ambient light and (c-d) 365-nm UV illuminations. (e-h) Microscopic photoluminescence images of CsPbBr₃ and CsPb₂Br₅ under (e-f) 473-nm laser (g-h) focused 365-nm UV illuminations. (i) Typical photoluminescence spectra of CsPbBr₃ and CsPb₂Br₅ powders. (j) Raman spectra of CsPbBr₃ and CsPb₂Br₅ powders at room temperature and 80 K. (k) Evolution of Raman spectrum when water was added to CsPbBr₃.

Figs. 1a-b show photographs of CsPbBr₃ and CsPb₂Br₅ powders. The color change from orange to white not only confirms a crystal phase transformation, but also indicates a potentially big increase in bandgap. However, when illuminated by a UV light (Figs. 1c-d), CsPb₂Br₅ powders

emit bright green light. In contrast, CsPbBr₃ remains almost dark, emitting weak light. The difference is still distinguishable under an optical microscope when excited by a 473-nm laser (Figs. 1e-f): a strong green emission is only observed in CsPbBr₃ from the laser excitation spot, while for CsPb₂Br₅, a large region surrounding the laser excitation spot becomes bright. More importantly, it appears that bluish green emission comes from the edges of individual CsPb₂Br₅ crystals. This difference in luminescence images can be seen more clearly when both CsPbBr₃ and CsPb₂Br₅ powders are under a stronger UV illumination (Figs. 1g-h): light comes from whole CsPbBr₃ crystals uniformly while only edges of CsPb₂Br₅ becomes bright.

The difference in emission wavelength is also revealed by their spectra in Fig. 1i. CsPbBr₃ exhibits two peaks at 528 and 542 nm²⁵, but CsPb₂Br₅ has a broad peak blue shifted from the PL of CsPbBr₃. This phase change was confirmed by Raman spectroscopy^{26, 27, 28}. Fig. 1j shows Raman spectra of CsPbBr₃ and CsPb₂Br₅ at room temperature and 80 K. The spectra of the two compounds can be distinguished easily at room temperature by the characteristic sharp lines of CsPb₂Br₅ at low wavenumbers versus the two-phonon mode of CsPbBr₃ at 309 cm⁻¹ and by strong double peaks of CsPbBr₃ at 25 cm⁻¹ at low temperature^{26, 27, 28}. The fast transition from CsPbBr₃ to CsPb₂Br₅ can also be seen from in-situ Raman in Fig. 1k.

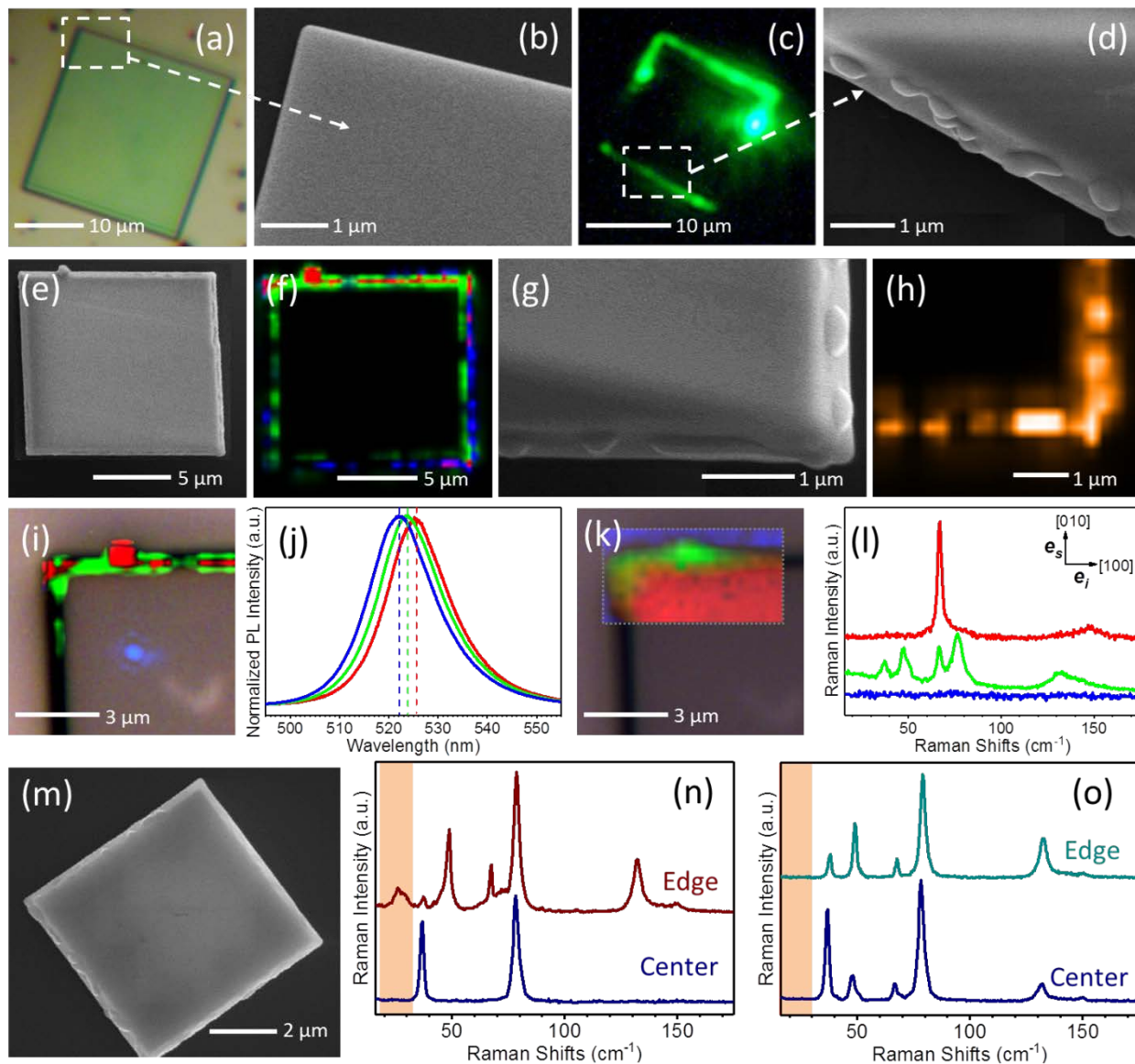


Fig. 2. Identification of edge emission in CsPb_2Br_5 microplatelets using PL, SEM and Raman. (a) Optical and (b) SEM images of a CsPb_2Br_5 platelet that shows no PL. (c) Photoluminescence image of a 2nd CsPb_2Br_5 platelet when excited by a 473-nm laser in the center. (d) SEM of bright edge of the platelet in (c). (e-l) SEM, PL and Raman characterizations of a 3rd CsPb_2Br_5 platelet. (e) SEM and (f) confocal photoluminescence mapping. (g) SEM image and (h) photoluminescence intensity mapping of low right corner of the platelet. (i-l) Confocal photoluminescence and Raman mappings of top left corner of the platelet. (j) Three PL modes used for PL imaging in (f) and (i). (l) Three Raman

modes for the mapping in (k). (m-n) SEM and low-temperature Raman indicates co-existence of CsPbBr₃ and polycrystalline CsPb₂Br₅ in a luminescent bump of a 4th CsPb₂Br₅ platelet. (o) The absence of CsPbBr₃ Raman in low-temperature Raman scattering of a luminescent bump in a 5th platelet.

The apparent display of bright edges doesn't necessarily guarantee that light emission originates from the edges, it could simply be a result of edge light scattering and wave guiding of photoluminescence in CsPb₂Br₅ platelets as can be found in a luminescent solar concentrator²⁹. To find out the exact source for the edge emission, we prepared CsPb₂Br₅ platelets with very flat and clean top surfaces. Square-shaped thin microplatelets were scooped from the surface of CsPb₂Br₅ synthesis water solution and dried by N₂ blow in air⁸. Two types of platelets were observed under laser or UV excitation. The first type showed no photoluminescence at all. Figs. 2a-b show optical and SEM images of such "dark" platelet: both edges and top surface are extremely smooth. Fig. 2c shows the other type of platelet where some locations of edges are bright but the body of the platelet is dark under laser excitation. Fig. 2d reveals that bright edges are decorated with individual nanobumps while dark edges are smooth without any bumps as in Fig. 2b. These new observations lead us to conclude that CsPb₂Br₅ is a wide bandgap semiconductor and transparent to visible light; bright edge emissions come from nanobumps on the edges.

To identify the structure and composition of the emitting edges, we combined micro-PL and micro-Raman to probe individual bumps. Figs. 2e-j show SEM and confocal PL mapping of a CsPb₂Br₅ platelet, a good overlap between PL mapping and SEM image confirms these bumps as the source for the edge emission. To further identify the bumps and their relationship to the CsPb₂Br₅ platelets, we performed a Raman mapping of the same top-left corner of the platelet as the one shown in the PL mapping in Fig. 2i. Here a 632.8-nm laser was used to eliminate strong PL background. In addition, Raman spectra were recorded in a scattering configuration that selects only two B_{2g} phonon lines in good single crystals²⁸. The Raman mapping in Fig. 2k reveals two distinct regions: a green region from the edge defined by a complete (depolarized) Raman spectrum (green) in Fig. 2(l) and red inner region characterized by two B_{2g} peaks. The

strongly polarized B_{2g} -spectra in the inner region indicate the good single crystal quality of the CsPb_2Br_5 platelet. Conversely, the emergence of all active modes indicates the presence of multiple CsPb_2Br_5 domains with different crystal orientations, i.e., polycrystalline CsPb_2Br_5 . An excellent spatial and intensity overlap between Raman and PL mappings implies that polycrystalline CsPb_2Br_5 is the main body of PL active bumps. Figs. 2m-o shows low temperature Raman spectra from similar bumps in two other platelets. A weak CsPbBr_3 Raman feature at 25 cm^{-1} can be seen in Fig. 2o, indicating co-existence of CsPbBr_3 and polycrystalline CsPb_2Br_5 , while no CsPbBr_3 Raman is observed in Fig. 2o.

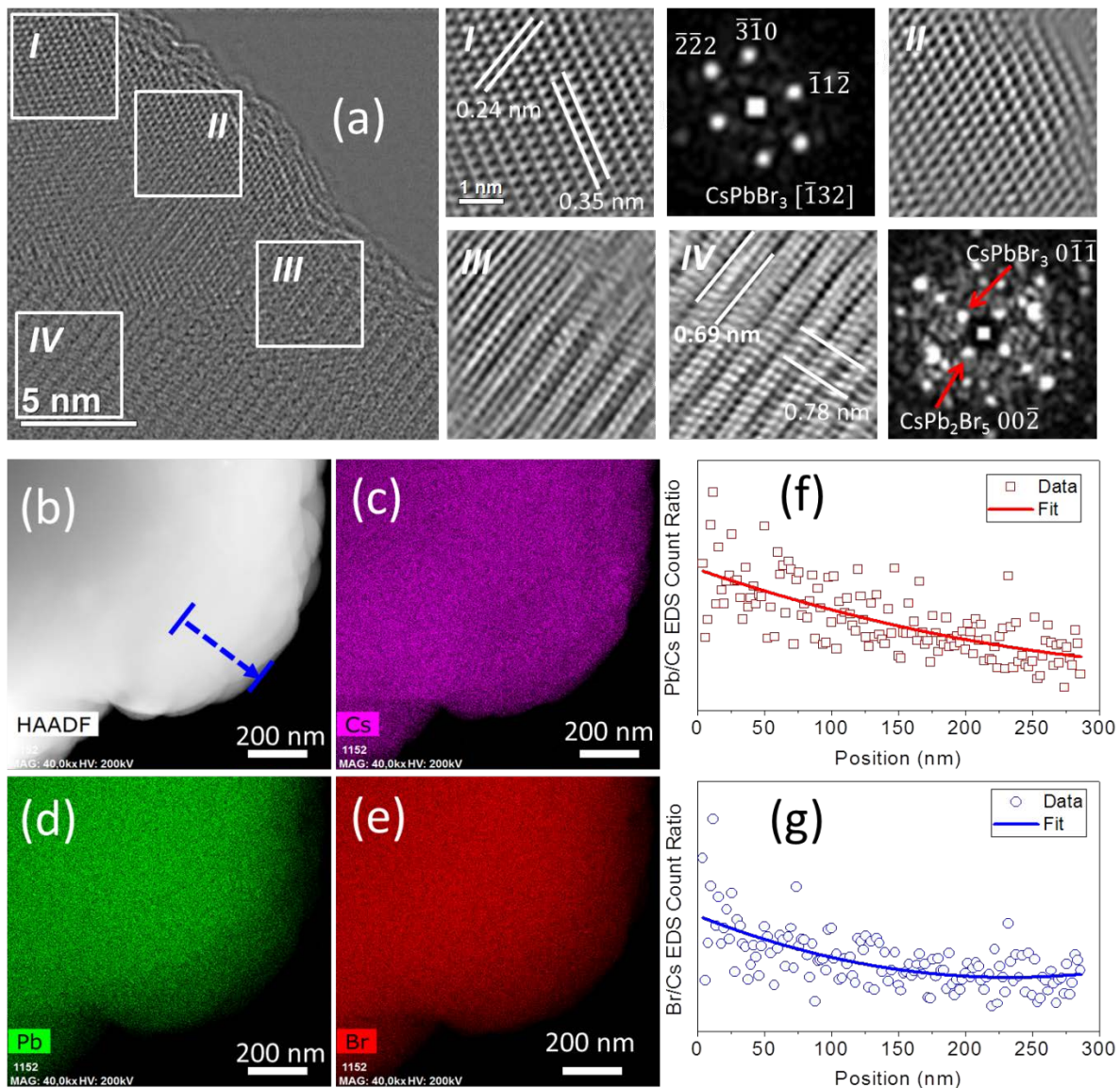


Fig. 3. Transmission electron microscopy (TEM) and energy-dispersive X-ray spectroscopy (EDS) investigations of a bump in a CsPb_2Br_5 platelet. (a) TEM phase image of the tip of the bump. Close-up and filtered sections of the phase images as indicated by regions I-IV; FFT electron diffraction patterns of the lattice in I and IV. (b) High angle annular dark field (HAADF) scanning TEM image of the bump. (c-e) EDS Cs, Pb and Br elemental mappings of the bump. (f-g) Pb/Cs and Br/Cs EDS count ratios along the line indicated in (b) and based on the Cs, Pb and Br mappings from (c) to (e).

The existence of both CsPbBr_3 and CsPb_2Br_5 in the same bumps can be most directly observed with atomic-resolution low dose aberration-corrected TEM and exit wave reconstruction (EWR)^{30, 31}. The use of low dose allows preserving the synthesized sample without beam alteration and thus the corresponding images represent the genuine structure. A dose of $30 \text{ e}/\text{\AA}^2\text{s}$ or lower was used here. Fig. 3a shows phase image of a bump near the surface. Also shown are selected regions I through IV and electron diffraction patterns of regions I and IV. Clearly, this whole region is not a single crystal lattice. The regions I and II can be clearly identified as CsPbBr_3 , but regions III and IV exhibit distorted lattice, can be hardly identified as pure CsPbBr_3 or CsPb_2Br_5 . For example, region IV can only be identified as a mixture of CsPbBr_3 and CsPb_2Br_5 . Because the base of the bump is single crystal CsPb_2Br_5 , we believe that TEM reveals a gradual phase transition from CsPb_2Br_5 to CsPbBr_3 . Such transition can also be qualitatively confirmed by energy-dispersive X-ray spectroscopy (EDS) elemental mapping in Fig. 3b-e. From the inner CsPb_2Br_5 region to the surface, Cs intensity remains almost constant, but Pb shows a rapid drop near the surface. Br intensity also drops, but not as fast as Pb near the surface. Such relative ratios of Pb and Br to Cs EDS counts are confirmed by analysis shown in Figs. 3f-g. These observations agree with the expectation from the transition from CsPb_2Br_5 to CsPbBr_3 : Pb/Cs ratio will decrease from 2 in CsPb_2Br_5 to 1 in CsPbBr_3 , while the Br/Cs ratio should decrease from 5 in CsPb_2Br_5 to 3 in CsPbBr_3 .

The identification of small amounts of CsPbBr_3 by TEM agrees with the Raman study in Fig. 2n, where Raman signatures of both CsPbBr_3 and CsPb_2Br_5 are observed. The absence of CsPbBr_3

Raman in Fig. 2o certainly indicates a negligible amount of CsPbBr₃ compared to CsPb₂Br₅. To obtain a lower limit of CsPbBr₃, we chose lasers with energy close to the PL peak so that Raman can be resonantly enhanced. An additional benefit of this approach is that photoluminescence and Raman can be captured in the same spectrum so that the contribution of CsPbBr₃ to the photoluminescence can be more accurately quantified. Fig. 4a shows a spectrum of the big bump in Figs. 2e, 2f and 2i by a 532-nm laser: a CsPbBr₃ Raman line at 309 cm⁻¹ can be clearly seen on the strong PL shoulder, the Raman of CsPb₂Br₅ at 133 cm⁻¹ appears relative weak due to even stronger PL background. This combined PL and Raman spectrum reveals a possible contribution of CsPbBr₃ to the PL and proves itself as a highly sensitive technique compared to a quick Raman mapping in Figs. 2k-l. Similar combined PL and Raman can also be achieved by a shorter wavelength laser. Fig. 4b shows a spectrum from a bump of another CsPb₂Br₅ microplatelet excited by a 473-nm laser. Despite a very strong luminescence, a clear CsPbBr₃ Raman peak at 309 cm⁻¹ can still be seen in the close-up view.

With this sensitive combined Raman/PL technique, we now show more cases that CsPbBr₃ alone cannot explain the bright photoluminescence, and polycrystalline CsPb₂Br₅ is carrying another highly luminescence agent even though its single crystal is totally transparent. Let's first take another look at CsPbBr₃ to CsPb₂Br₅ transition in water. Figs. 4c-f show in-situ PL imaging of the transition under the UV illumination. A big CsPbBr₃ single crystal can be easily recognized by its green body emission. The crystal was dissolved into several smaller pieces and gradually disappeared after several minutes. In the meantime, bright spots with bluish green color began to emerge from previous dark regions. This observation has given us very important information: these bright spots are not the initial CsPbBr₃ and cannot be made of CsPbBr₃, they must be polycrystalline CsPb₂Br₅. This assumption can be quickly confirmed. Figs. 4g-j show photoluminescence and Raman from these bright spots in water. A strong Raman peak at 133 cm⁻¹ confirms CsPb₂Br₅, no Raman peak of CsPbBr₃ at 309 cm⁻¹ is found. Note that the Raman spectrum in Figs. 4h-i is similar to that in Fig. 4b in terms of dynamic range and signal to noise ratio, if CsPbBr₃ is responsible for the bright emission, it must exhibit the characteristic Raman peak. The same conclusion can be made from the comparison between Fig. 4j and 4a when PL and Raman were excited by the 532-nm laser.

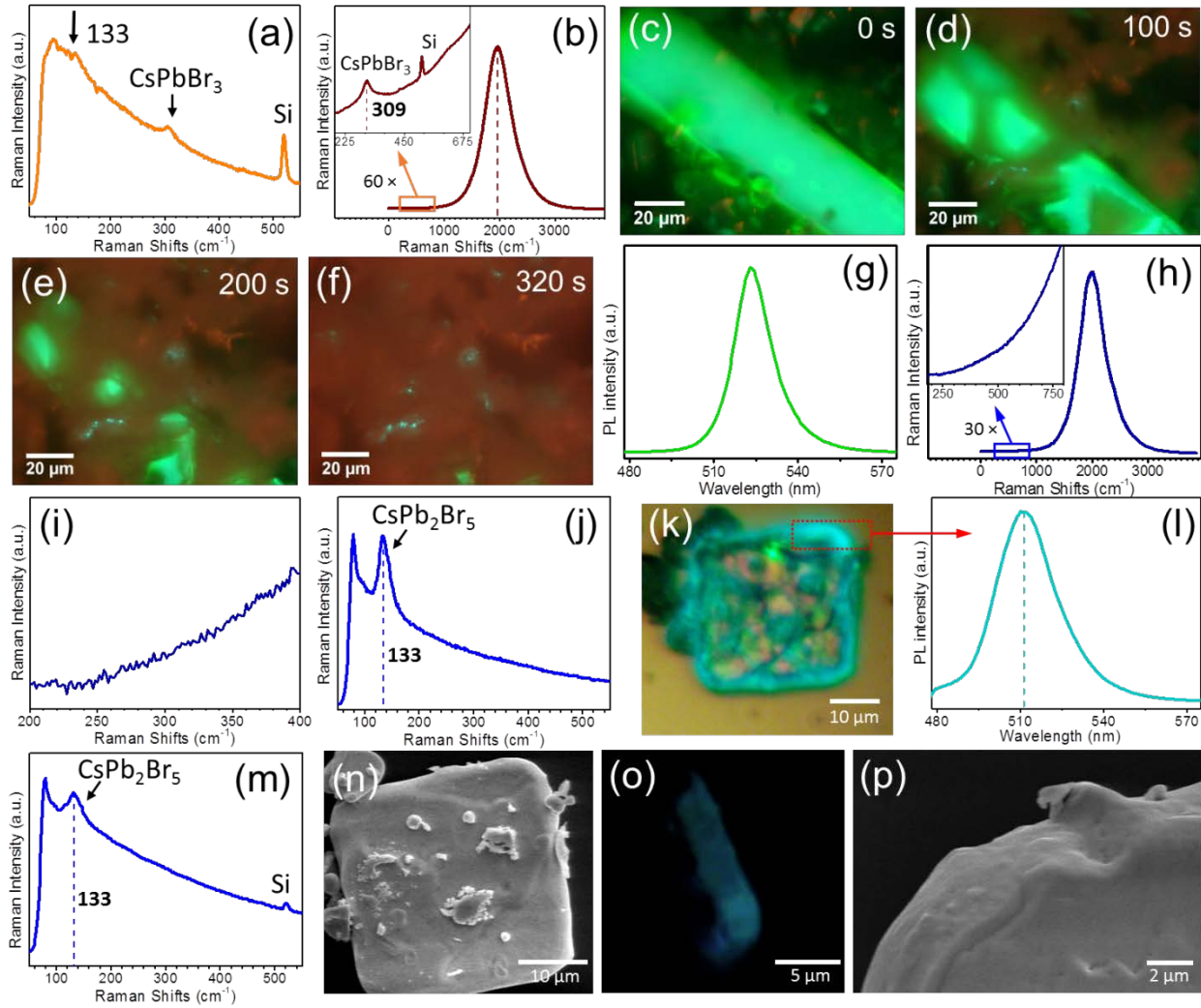


Fig. 4. PL and Raman spectroscopy of polycrystalline CsPb_2Br_5 . (a) Combined Raman and PL spectrum of the big bump of the CsPb_2Br_5 platelet in Figs. 2e,2i and 2k excited by a 532-nm laser. (b) Combined Raman and PL spectrum of a bump of a 5th CsPb_2Br_5 platelet excited by a 473-nm laser. (c-f) In-situ PL imaging of the dissolution of a large CsPbBr_3 crystal and formation of bright luminescent polycrystalline CsPb_2Br_5 spots. (g) Typical PL spectrum of a bright spot of CsPb_2Br_5 in water. (h-j) Combined Raman and PL spectra of a luminescent spot of CsPb_2Br_5 in water excited by (h-i) the 473-nm laser and (j) the 532-nm laser. (i) and inset of (h): zoomed-in spectrum near 309 cm^{-1} . (k) PL imaging, (l) PL spectrum, (m) Raman spectrum and (n) SEM of a CsPb_2Br_5 platelet. PL was

excited by 473-nm laser and Raman was excited by 532-nm laser. (o) PL and (p) SEM image of edge of another CsPb₂Br₅ platelet.

We applied the same combined Raman/PL technique to the bright CsPb₂Br₅ in Figs. 1f and 1h again. Fig. 4k shows the PL image of a CsPb₂Br₅ crystal. As expected, this edge emission has a broad shorter wavelength centered at 511 nm (Fig. 4l). Raman spectrum from the same spot exhibits a strong CsPb₂Br₅ peak at 133 cm⁻¹ but without any sign of CsPbBr₃ peak at 309 cm⁻¹ (Fig. 4m). Based on the same reason, we conclude that the contribution of CsPbBr₃ to the photoluminescence is negligible, in other words, polycrystalline CsPb₂Br₅ is responsible for the strong PL. This shorter wavelength emission and lack of CsPbBr₃ is due to different edge morphology: SEM in Fig. 4n shows relatively smooth edges without large bumps. A direct edge emission and edge morphology can be found in Figs. 4o-p.

Now we have three types of CsPb₂Br₅ that show edge emissions: bumps on the edges of platelets (Fig. 2), immersed in water (Fig. 4c-j), and no bump but with relatively “rough” surfaces (Fig. 1f-h, Fig. 4k-p). Their different morphologies and compositions are due to slightly different drying processing. For the platelets with bumps in Fig. 2, they were scooped with a silicon substrate from the water surface and were blow dried by N₂ after they emerged to the surface from the precipitates at the bottom. In this case, some water will be left on the edges, and metal halide ions in the water will precipitate as water dries up. CsPbBr₃ nanocrystals might form on the top of polycrystalline CsPb₂Br₅; because CsPbBr₃ has a high solubility in water, it cannot crystallize until the platelet is dried. For this reason, the bright luminescent spots must come from polycrystalline CsPb₂Br₅ in water, in agreement with the combined Raman/PL investigation. On the other hand, if CsPbBr₃ nanocrystals can be embedded in CsPb₂Br₅, we should already have observed them inside CsPb₂Br₅ platelets and found their corresponding body emission^{32, 33}. CsPb₂Br₅ platelets with relatively rough surface but without bumps are white precipitates, they were collected and then washed by diethyl ether for three times before they were dried in a furnace at 60 degrees for 12 hours. Rinsing with diethyl ether is a typical procedure to remove residual water from a crystal surface; as a result, no water droplets were left on the edges and no bumps were formed.

Let us discuss the possible causes for PL in polycrystalline CsPb₂Br₅. Many different types of defects can be created on the edges between the boundaries of CsPb₂Br₅ nanocrystals, including vacancies, interstitials and distorted bonds. Br vacancies can be excluded because a recent DFT study shows that Br vacancies in CsPb₂Br₅ monolayers create shallow levels at 0.12 – 0.25 eV below the conduction band³⁴. Self-trapped excitons are another contender but they can also be excluded because the laser energies are too small to create free excitons in CsPb₂Br₅. We believe that clusters of corner sharing PbBr₆ octahedrons on the edges are responsible for the bright luminescent edge states. The bandgaps of perovskites are mainly determined by lead halide octahedrons and their framework. The distorted lattices or variation of the octahedral tilting angles between octahedrons in these macro-molecules made of individual PbBr₆ molecules will result in a slightly larger bandgap than that of fully connected PbBr₆ network, i.e., CsPbBr₃³⁵.

Our discovery and understanding of luminescent states on the edges of wide bandgap CsPb₂Br₅ single crystals explain many seemingly conflicting observations. For large and even millimeter size crystals, transparent non-emissive plates of CsPb₂Br₅ are more convenient to observe than possible edge emission; for small crystals especially submicron-sized particles or platelets, it is difficult to distinguish edge emission from body emission. In some cases, CsPb₂Br₅ could have potential “contamination” from CsPbBr₃ nanocrystals^{13, 14, 15}. More research is clearly needed to verify the origin of luminescent deep level edge states. Metal halide octahedrons are the basic building blocks of perovskites with any dimensionality and understanding properties of clusters of corner sharing octahedrons is essential to the understanding of defects and defect states of any perovskites. Because such luminescent properties have already found applications in making high efficiency defect-tolerant solar cells and light emitting diodes, our discoveries will accelerate more understanding and applications of perovskites.

References:

1. Zhao YX, Zhu K. Organic-inorganic hybrid lead halide perovskites for optoelectronic and electronic applications. *Chemical Society Reviews* **45**, 655-689 (2016).
2. Huang J, Yuan Y, Shao Y, Yan Y. Understanding the physical properties of hybrid perovskites for photovoltaic applications. *Nat Rev Mater* **2**, 17042 (2017).
3. Xiao JW, *et al.* The Emergence of the Mixed Perovskites and Their Applications as Solar Cells. *Adv Energy Mater* **7**, 1700491 (2017).
4. Zhu HM, *et al.* Lead halide perovskite nanowire lasers with low lasing thresholds and high quality factors. *Nat Mater* **14**, 636-U115 (2015).
5. Lin HR, Zhou CK, Tian Y, Siegrist T, Ma BW. Low-Dimensional Organometal Halide Perovskites. *ACS Energy Lett* **3**, 54-62 (2018).
6. Blancon JC, *et al.* Extremely efficient internal exciton dissociation through edge states in layered 2D perovskites. *Science* **355**, 1288-1291 (2017).
7. Kuznetsova IY, Kovaleva IS, Fedorov VA. Interaction of lead bromide with cesium and cadmium bromides. *Russ J Inorg Chem* **46**, 1730-1735 (2001).
8. Rodova M, Brozek J, Knizek K, Nitsch K. Phase transitions in ternary caesium lead bromide. *J Therm Anal Calorim* **71**, 667-673 (2003).
9. Zhang XL, *et al.* All-Inorganic Perovskite Nanocrystals for High-Efficiency Light Emitting Diodes: Dual-Phase CsPbBr₃-CsPb₂Br₅ Composites. *Adv Funct Mater* **26**, 4595-4600 (2016).
10. Wang KH, Wu L, Li L, Yao HB, Qian HS, Yu SH. Large-Scale Synthesis of Highly Luminescent Perovskite-Related CsPb₂Br₅ Nanoplatelets and Their Fast Anion Exchange. *Angew Chem-Int Edit* **55**, 8328-8332 (2016).
11. Li GP, *et al.* Shape and phase evolution from CsPbBr₃ perovskite nanocubes to tetragonal CsPb₂Br₅ nanosheets with an indirect bandgap. *Chem Commun* **52**, 11296-11299 (2016).
12. Tang XS, *et al.* Perovskite CsPb₂Br₅ Microplate Laser with Enhanced Stability and Tunable Properties. *Adv Opt Mater* **5**, 1600788 (2017).
13. Ruan L, Shen W, Wang A, Xiang A, Deng Z. Alkyl-Thiol Ligands Induced Shape and Crystalline Phase Controlled Synthesis of Stable Perovskite-Related CsPb₂Br₅ Nanocrystals at Room Temperature. *The Journal of Physical Chemistry Letters* **8**, 3853-3860 (2017).
14. Li PZ, *et al.* Novel synthesis and optical characterization of CsPb₂Br₅ quantum dots in borosilicate glasses. *Mater Lett* **209**, 483-485 (2017).
15. Qin CJ, Matsushima T, Sandanayaka ASD, Tsuchiya Y, Adachi C. Centrifugal-Coated Quasi-Two-Dimensional Perovskite CsPb₂Br₅ Films for Efficient and Stable Light-Emitting Diodes. *J Phys Chem Lett* **8**, 5415-5421 (2017).
16. Lv JF, Fang LL, Shen JQ. Synthesis of highly luminescent CsPb₂Br₅ nanoplatelets and their application for light-emitting diodes. *Mater Lett* **211**, 199-202 (2018).
17. Han C, *et al.* Tunable luminescent CsPb₂Br₅ nanoplatelets: applications in light-emitting diodes and photodetectors. *Photonics Res* **5**, 473-480 (2017).
18. Dursun I, *et al.* CsPb₂Br₅ Single Crystals: Synthesis and Characterization. *ChemSusChem* **10**, 3746-3749 (2017).
19. Zhang Z, Zhu Y, Wang W, Zheng W, Lin R, Huang F. Growth, characterization and optoelectronic applications of pure-phase large-area CsPb₂Br₅ flake single crystals *Journal of Materials Chemistry C* **6**, 446-451 (2018).
20. Palazon F, *et al.* From CsPbBr₃ Nano-Inks to Sintered CsPbBr₃-CsPb₂Br₅ Films via Thermal Annealing: Implications on Optoelectronic Properties. *J Phys Chem C* **121**, 11956-11961 (2017).
21. Qiao B, *et al.* Water-resistant, monodispersed and stably luminescent CsPbBr₃/CsPb₂Br₅ core-shell-like structure lead halide perovskite nanocrystals. *Nanotechnology* **28**, 445602 (2017).

22. Balakrishnan SK, Kamat PV. Ligand Assisted Transformation of Cubic CsPbBr₃ Nanocrystals into Two-Dimensional CsPb₂Br₅ Nanosheets. *Chem Mater* **30**, 74–78 (2017).
23. Stoumpos CC, *et al.* Crystal Growth of the Perovskite Semiconductor CsPbBr₃: A New Material for High-Energy Radiation Detection. *Cryst Growth Des* **13**, 2722-2727 (2013).
24. Dong QF, *et al.* Electron-hole diffusion lengths > 175 μ m in solution-grown CH₃NH₃PbI₃ single crystals. *Science* **347**, 967-970 (2015).
25. Stoumpos CC, *et al.* Ruddlesden-Popper Hybrid Lead Iodide Perovskite 2D Homologous Semiconductors. *Chem Mat* **28**, 2852-2867 (2016).
26. Cha JH, *et al.* Photoresponse of CsPbBr₃ and Cs₄PbBr₆ Perovskite Single Crystals. *J Phys Chem Lett* **8**, 565-570 (2017).
27. Yaffe O, *et al.* Local Polar Fluctuations in Lead Halide Perovskite Crystals. *Phys Rev Lett* **118**, 136001 (2017).
28. Hadjiev VG, *et al.* Phonon fingerprints of CsPb₂Br₅ single crystals. *submitted*, (2018).
29. Zhou Y, *et al.* Colloidal carbon dots based highly stable luminescent solar concentrators. *Nano Energy* **44**, 378–338 (2018).
30. Kisielowski C, *et al.* Real-time sub-Angstrom imaging of reversible and irreversible conformations in rhodium catalysts and graphene. *Phys Rev B* **88**, 024305 (2013).
31. Calderon HA, Kisielowski C, Specht P, Barton B, Godinez-Salomon F, Solorza-Feria O. Maintaining the genuine structure of 2D materials and catalytic nanoparticles at atomic resolution. *Micron* **68**, 164-175 (2015).
32. Chen X, *et al.* Centimeter-Sized Cs₄PbBr₆ Crystals with Embedded CsPbBr₃ Nanocrystals Showing Superior Photoluminescence: Nonstoichiometry Induced Transformation and Light-Emitting Applications. *Adv Funct Mater* DOI: **10.1002/adfm.201706567**, (2018).
33. De Bastiani M, *et al.* Inside Perovskites: Quantum Luminescence from Bulk Cs₄PbBr₆ Single Crystals. *Chem Mat* **29**, 7108-7113 (2017).
34. Iyikanat F, Sari E, Sahin H. Thinning CsPb₂Br₅ perovskite down to monolayers: Cs-dependent stability. *Phys Rev B* **96**, 155442 (2017).
35. Pedesseau L, *et al.* Advances and Promises of Layered Halide Hybrid Perovskite Semiconductors. *ACS Nano* **10**, 9776-9786 (2016).